ISSN 1995-0780, Nanotechnologies in Russia, 2020, Vol. 15, No. 1, pp. 112–120. © Pleiades Publishing, Ltd., 2020.
Russian Text © The Author(s), 2020, published in Rossiiskie Nanotekhnologii, 2020, Vol. 15, No. 1, pp. 125–134.

NANOBIOMEDICINE AND NANOPHARMACEUTICALS

Local Atomic and Electronic Structures of Superparamagnetic Nanoparticles Based on Iron Oxides for Local Hyperthermia in Oncology

Z. M. Gadzhimagomedova[a,*], O. E. Polozhentsev[a], E. A. Kuchma[a,b], M. A. Soldatov[a], D. Yu. Kirsanova[a], A. Yu. Maximov[b], and A. V. Soldatov[a]

[a] *The Smart Materials Research Institute, Southern Federal University, Rostov-on-Don, 344090 Russia*
[b] *National Medical Research Centre for Oncology, Ministry of Health of the Russian Federation, Rostov-on-Don, 344019 Russia*
**e-mail: zaira31may@gmail.com*

Received May 8, 2020; revised May 31, 2020; accepted June 1, 2020

Abstract—Iron oxide-based superparamagnetic nanoparticles (Fe_3O_4) are obtained using the solvothermal synthesis. Both the pure nanoparticles of Fe_3O_4 and nanoparticles doped by samarium and gadolinium are obtained to manipulate their characteristics. The materials were investigated using X-ray diffraction, X-ray fluorescence, vibrating-sample magnetometry, electron microscopy, electron diffraction, and FT-IR spectroscopy. The nanoparticles have the average size of about 22.3 nm, a crystal lattice of magnetite, and superparamagnetic characteristics at room temperature. Based on the FT-IR spectroscopy, all the synthesized nanoparticles included in their composition a polyethylene glycol coating. The hyperthermic characteristics (SAR and ILP) are determined for the obtained nanoparticles in an alternating magnetic field (AMF). The promising prospects of using the discussed superparamagnetic nanoparticles based on iron oxide particles doped by the atoms of the rare-earth elements for the local magnetic hyperthermia are shown.

DOI: 10.1134/S1995078020010176

INTRODUCTION

The local magnetic hyperthermia with the use of magnetic nanoparticles (MNPs) is among the promising modalities of tumor therapy due to its selective heating effect on the local tissue region and compatibility with the conventional treatment therapies for malignant neoplasms. Local magnetic hyperthermia is an address delivery of MNPs to the target tissue (malignant tumor) and their local heating in the dissipation region by applying an external alternating magnetic field (AMF) [1–3]. The target tissue exposed to high temperatures is either destroyed (thermal ablation at temperatures above 47°C) or becomes more susceptible to other treatment methods (thermal activation in the temperature range of 41 to 45°C).

The effectiveness and applicability of the local magnetic hypothermia can be improved based on nanotechnologies by creating the biocompatible and nontoxic nanomaterials and modifying the MNP surfaces using the antitumor drugs, visualization tools, and vectors for the targeted transport to the tumor to enhance their reliability and the cytotoxic effect on the tumor [4–6]. Advances in this field will lead to the design of novel biocompatible target MNPs that will need to be assessed for the possibility of their use with the local magnetic hyperthermia method and identification of their optimal characteristics. Successful development of magnetic hyperthermia will depend on finding the solutions to a number of problems. Firstly, it is important to improve the methods of preparing the nanoparticles' colloidal suspensions with sufficiently large deposition by mass in an AMF of a moderate amplitude. This will allow reducing the dose of nanoparticles sufficiently to achieve a positive treatment effect. Ideally, it is desirable to find a way for heating the small tissue volumes locally to suppress tiny but fatal neoplasms. Next, it is necessary to ensure the creation of an AMF of sufficient amplitude with the needed spatial dissipation in the given body region and guaranteed safety against electric shock. Finally, it is important to know how to control the exposure itself by establishing the amplitude and frequency of the magnetic field, magnetic and geometric parameters of the nanoparticles, and duration and time period of the exposure taking into account the electrodynamic and thermal parameters of the medium. It is desirable to be able to control the spatial and temporal distribution of the temperature in the exposure region.

The magnetic properties and heating characteristics of the nanoparticles are largely determined by their chemical composition and structure. The saturation magnetization (M_s) of the nanoparticles widely used for biomedical purposes is normally as follows for

metallic nanoparticles: Fe ~300 emu/g, Co ~250 emu/g, Ni ~200 emu/g, magnetite ~92 emu/g, maghemite ~80 emu/g, and manganese ferrite $MnFe_2O_4$ ~110 emu/g [7–10]. It is possible to obtain MNPs with higher heating characteristics by manipulating the chemical composition and structure of the nanoparticles.

Doping the nanoparticles by nonmagnetic Zn^{2+} ions is one of the methods used to improve their magnetic properties. At $x \le 0.4$, the Zn^{2+} ions occupying the tetrahedral voids decrease the antiferromagnetic interactions between the Fe^{3+} ions at sites *A* and *B*, which leads to an increase in the degree of magnetization for the Zn-doped system [10, 11]. At the higher Zn^{2+} doping levels, antiferromagnetic interactions between Fe^{3+} ions at each *B*-site become dominant, while the resultant magnetization decreases. The effect of doping the rare earth elements (Gd, Eu, Sm, etc.) on the magnetic properties has also been studied. The gadolinium Gd^{3+} ion features seven unpaired electrons on 4*f*-orbitals, large magnetic moment (μ_B = 6.8 μB/atom), and demonstrates a long spin relaxation time ($T_1 \sim 10^{-9}$ s) at the magnetic field strength normally used in MRI (magnetic resonance imaging) [10, 11]. Spherical magnetite nanoparticles doped with Gd (10%) (Fe_3O_4:Gd (10%)) feature a higher degree of magnetization and the specific absorption rate (SAR), which is twice as large as in the undoped analog of Fe_3O_4 nanoparticles with values of 438.6 and 189.6 W/g, respectively [10]. These findings demonstrate the importance of manipulating the chemical composition of magnetic materials to increase magnetization, which results in the improved MNP heating characteristics for magnetic hyperthermia.

The effectiveness of magnetic hyperthermia is determined by the values of the SAR or intrinsic loss power (ILP) of the nanoparticles, which depend primarily on the physicochemical and magnetic properties of the nanoparticles and parameters of the external magnetic fields applied [3, 5]. The normalized parameter of magnetic hyperthermia is an ILP value not dependent on the parameters of the external magnetic field in various experiments. Overall, the ILP values vary between 1 and 4 nH m^2/kg [6, 10].

The M_s and hyperthermic ILP properties of the nanoparticles of magnetite widely used in biomedicine are normally as follows: M_s = 40–80 emu/g and ILP = 0.1–1.0 nH m^2/kg [6, 10]. The strategy for doping the MNPs with various chemical elements in a small concentration is one of the ways of improving the magnetic and hyperthermic properties.

Studies of the hyperthermic properties of magnetite MNPs doped by the transition and rare-earth elements [12–16] are reported in the literature. Depending on the degree of Mn and Zn codoping, magnetite MNPs of 10 to 15 nm feature M_s between 66 and 81 emu/g and ILP values between 0.1 nH m^2/kg (Zn–Fe_3O_4) and 1 nH m^2/kg (Mn–Fe_3O_4) [12]. In [13] the authors report cobalt-doped MNPs ($Co_{0.6}Fe_{2.4}O_4$) of 8 nm with M_s of 58.44 emu/g and ILP of 9.86 nH m^2/kg is reported. In [14] the authors report magnetite MNPs of ~20 nm doped by different amounts of Y^{3+} (0, 0.1, 1, and 10%) ions. The best results were obtained for Fe_3O_4 MNPs doped by 0.1% Y^{3+} ions (M_s = 69 emu/g, SAR = 194 W/g, and ILP = 1.85 nH m^2/kg). In [15] magnetite MNPs doped by (2%) Gd ($Gd_{0.02}Fe_{2.98}O_4$) ions ~13 nm in size with M_s ~ 66 emu/g and SAR = 36 W/g were obtained, which is four times as large as the ones in nondoped magnetite MNPs.

Doping magnetite MNPs by rare-earth metals (Gd, Sm, Eu, etc.) has a number of advantages. Rare-earth metals with incomplete 4*f*-electron shells features a large magnetic moment and strong ferromagnetic coupling compared to the 3*d*-transition metals. Thus, the gadolinium Gd^{3+} ion has seven unpaired electrons on 4*f*-orbitals and a large magnetic moment (μ_B = 6.8 μB/atom) and demonstrates an extra-long spin relaxation time at the magnetic field strength; it is commonly used as a contrast agent in MRI [15, 16]. In addition, reports are available that indicate that doping by Gd promotes a decrease in the Curie temperature of iron oxides, which can be exploited as the MNP self-deactivation mechanisms on attaining the therapeutic temperatures of 42 to 47°C [15]. These results demonstrate the importance of doping and manipulating the chemical composition of magnetic materials to enhance magnetization and improve the MNPs' heating characteristics for magnetic hyperthermia.

The aim of this study is to study the effect of doping MNPs by rare-earth elements (Sm and Gd) on the physicochemical and hyperthermic characteristics of the MNPs.

EXPERIMENTAL

The iron oxide-based superparamagnetic nanoparticles (Fe_3O_4) coated with polyethylene glycol (PEG-2000) were obtained using the solvothermal synthesis with ethylene glycol (EG) as the solvent and PEG as the surfactant. The following protocol was used to receive ~250–300 mg pure nanoparticles of Fe_3O_4 (POL01) magnetite:

—2 g of PEG-2000 (Sigma Aldrich) as a surfactant (stabilizer) was dissolved in 40 mL of EG (Alfa Aesar 99%), while being stirred continuously in a magnetic stirrer at a temperature of 50°C and speed of 1000 rpm until the transparent solution was formed;

—2.0 mmol of iron(II) chloride tetrahydrate ($FeCl_2 \cdot 6H_2O$) (M = 234.8427 g/mol, m = 0.470 g) and 4.0 mmol iron(III) chloride hexahydrate ($FeCl_3 \cdot 6H_2O$) (M = 270.2957 g/mol, m = 1.081 g) were added to the solution. To stabilize the electrostatic charge,

10.0 mmol of sodium acetate trihydrate ($CH_3COONa \cdot 3H_2O$) (M = 136.08 g/mol, m = 1.36 g) was further added to the mixture;

—the mixture was stirred in a magnetic stirrer at 50°C and 1000 rpm to form a homogenous brown solution;

—the resultant solution was transferred over to a 100 mL PTPE-lined vessel of the chemical reactor and sealed;

—the nanoparticles were crystallized in a Parr autoclave at 200°C for 20 h, with constant stirring in a magnetic stirrer (rotational speed 1000 rpm);

—next, the dispersion was cooled to room temperature;

—the resulting black precipitate was separated from the dispersion using the magnetic separation, rinsed several times with distilled water, and allowed to dry for a few hours in a drying chamber at 60°C.

At the second stage of obtaining the rare-earth elements (Sm (POL02), Gd (POL03))-doped nanoparticles, 2.0 mmol of iron(II) chloride tetrahydrate ($FeCl_2 \cdot 6H_2O$) was replaced with 0.4 mmol (10%) of samarium(III) chloride ($SmCl_3$ (POL02)) or 0.4 mmol (10%) gadolinium(III) chloride ($GdCl_3$ (POL03)) to achieve a 10% concentration of the rare-earth elements.

The dried black powder was further utilized to analyze the crystal structure, the size and shape of the nanoparticles, chemical composition, and the magnetic properties. An aqueous colloidal suspension with a concentration of at least 15 mg/mL was used to measure the hyperthermic characteristics of the obtained nanoparticles. Such a concentration was chosen in order to note the significant rise in temperature and estimate the speed of the temperature change at the initial instant of exposure to an AMF. The SAR parameter is linearly dependent on the nanoparticles' concentration and normalized to the mass of the nanoparticles. Such concentrations of nanoparticles are not for intravenous administration.

RESULTS AND DISCUSSION

The type of the crystal lattice and average size of the crystallites in the synthesized nanoparticles were determined using the X-ray diffraction (XRD) with a D2 PHASER diffractometer (Bruker Corp., Germany) (CuK_α radiation, λ = 1.5406 Å) at room temperature within 10°–90° based on the 2θ scale at the scan speed of 6 deg/min and step size of 0.02°. Figure 1 illustrates the diffractograms of the obtained nanoparticles. The diffractograms show the characteristic peaks on the axis 2θ: 18.3° (111), 30.1° (220), 35.5° (311), 37.0° (222), 43.1° (400), 53.5° (422), 57.0° (511), and 62.5° (440), which correspond to a structure of magnetite (Fe_3O_4) with a cubic inverse spinel structure and space group *Fd*3*m* composed of a cubic closely packed lattice of oxide ions; all the Fe^{2+} ions occupy half of the octahedral voids, while the Fe^{3+} ions are distributed evenly between the remaining octahedral and tetrahedral voids. The average size of the synthesized nanoparticles crystallites was calculated using the Debye Scherrer equation as 44.1 nm for pure magnetite (POL01), 14.4 nm for the samarium-doped nanoparticles (POL02), and 17.7 nm for the gadolinium-doped (POL03) nanoparticles.

The morphology and size of the synthesized nanoparticles were examined using the transmission electron microscopy (TEM) and electron diffraction with the Tecnai G2 Spirit BioTWIN electron microscope (FEI, United States). Figure 2a shows the TEM image of the samarium-doped magnetite nanoparticles (POL02) at ×200 magnification. These spherical particles average 22.3 nm in size. The hydrodynamic size of the nanoparticles and the distribution width of the particle size were determined by dynamic light scattering (DLS) with the particle size analyzer NANO-Flex (MicroTrac GmbH, Germany). Figure 2b presents the distribution histograms, which demonstrate that the average size of the nanoparticles is 246.1 ± 131.4 nm for POL01, 83.7 ± 55.3 nm (82.5%) for POL02, and 29.01 ± 10.96 nm for POL03.

According to the results of the X-ray fluorescence performed using an M4 Tornado spectrometer (Bruker Corp., Germany), the concentration of samarium relative to iron is 8.64 wt % or 3.33 at % in the nanoparticles (POL02) and the gadolinium concentration is 14.8 wt % or 5.81 at % in the gadolinium-doped nanoparticles (POL03).

The surface of the nanoparticles and the associated organic ligands PEG-2000 were investigated using the Fourier-transform infrared spectroscopy with the Vertex-70 spectrometer (Bruker Corp., Germany). Figure 3 shows the FT-IR spectra of the magnetite nanoparticles both not doped and doped by rare-earth elements (Sm and Gd). Such elements have two primary absorption bands at 570–540 and 330–380 cm^{-1}, which correspond to the vibrations of the Fe–O bonds in the tetrahedral and octahedral voids, respectively. In the doped nanoparticles, the positions of the peaks are slightly shifted to higher frequency domains, which is related to the presence in their composition of elements with a larger atomic weight and, consequently, to changes in the size of the magnetite space unit. Similarly, the characteristic vibrations of PEG-2000 were revealed by the FT-IR spectra at 1084 cm^{-1} (C–OH, stretching vibrations), 1426 cm^{-1} (C–H, bending vibrations), 1576 cm^{-1} (C=C, stretching vibrations), 2914 cm^{-1} (C–H, stretching vibrations), and other peaks. The occurrence of the characteristic PEG-2000 peaks in the FT-IR spectra of the synthesized nanoparticles (POL01–POL03) confirms the successful coating by PEG-2000 of the MNPs. The wide peak at 3400 cm^{-1} can be explained by the presence of –OH on the surface of the nanoparticles.

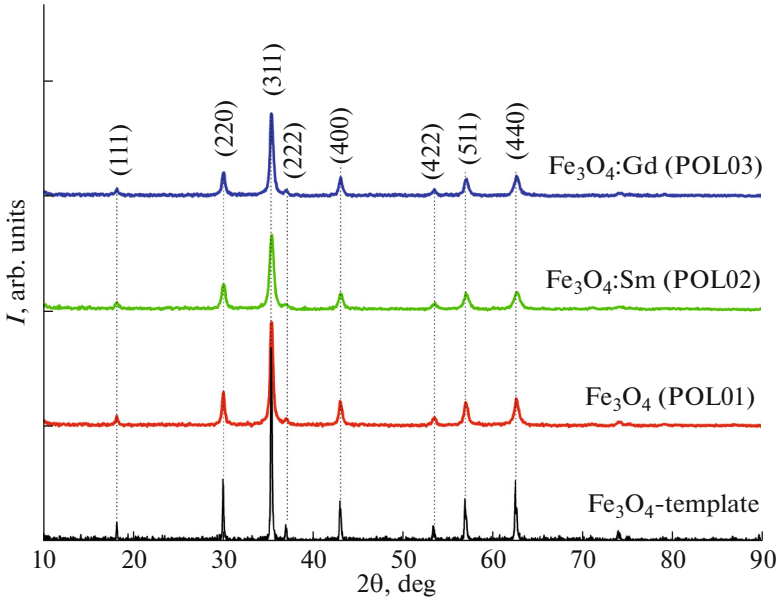

Fig. 1. (Color online) Diffractograms of the synthesized Fe_3O_4 (POL01), Fe_3O_4:Sm (POL02), and Fe_3O_4:Gd (POL03) nanoparticles coated with PEG-2000.

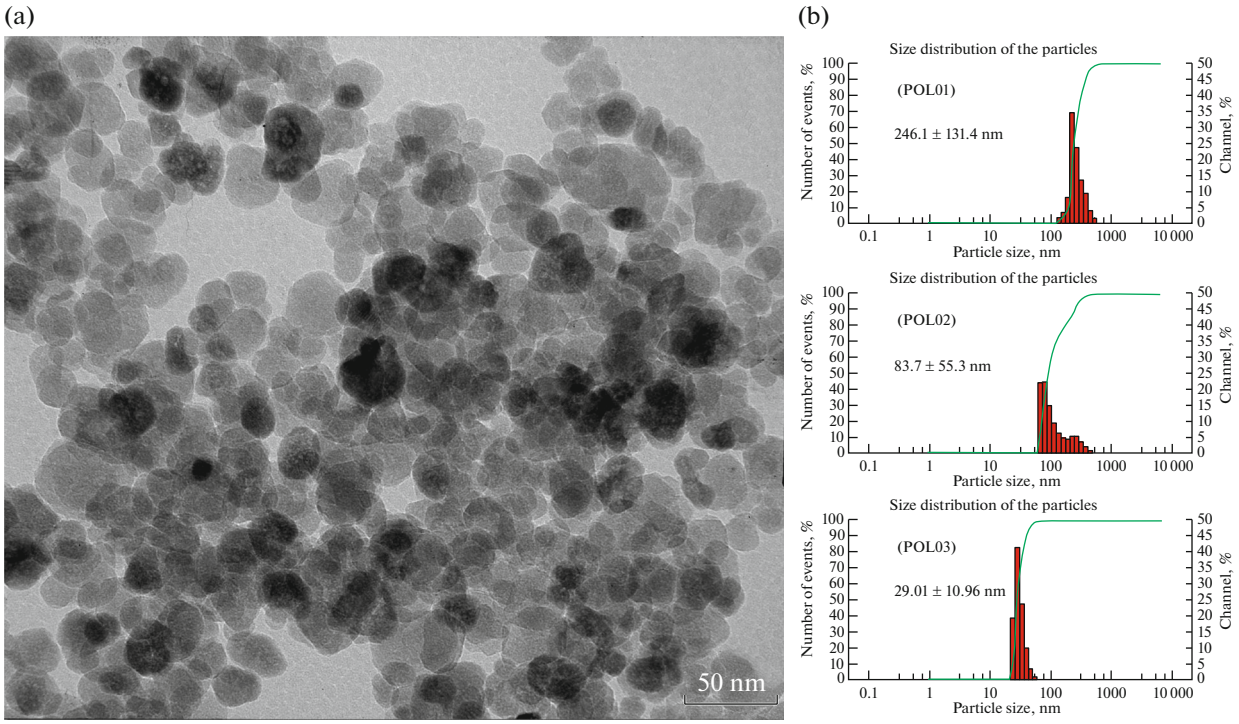

Fig. 2. (Color online) TEM image at ×200 magnification of (a) the samarium-doped magnetite nanoparticles (POL02), (b) histogram of the synthesized nanoparticles' hydrodynamic distribution by radius size.

A vibrating-sample magnetometer (VSM), model 7404 (Lake Shore Cryotronics, United States) served to determine the type of magnetic ordering and magnetic characteristics of the synthesized nanoparticles. Figure 4 represents the magnetization curves with hysteresis loops. The loop's visual representation allows determining the type of magnetic ordering and magnetic characteristics of the studied nanoparticles, such as M_s, remanence magnetization (M_r), and coercivity H_c. Pure magnetite nanoparticles coated

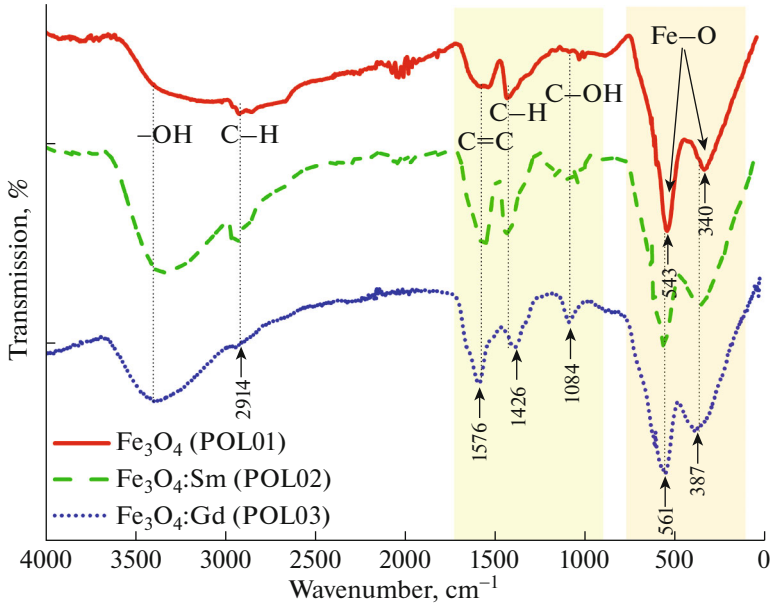

Fig. 3. (Color online) FT-IR spectra of Fe_3O_4 (POL01), Fe_3O_4:Sm (POL02), and Fe_3O_4:Gd (POL03) nanoparticles coated with PEG-2000.

with PEG-2000 featured M_s of 74 emu/g. The samarium-doped nanoparticles had a significantly higher M_s of 122 emu/g compared with pure nanoparticles; however, when doped by gadolinium, the nanoparticles displayed a lower M_s of 46 emu/g. The pure, gadolinium-doped, and samarium-doped nanoparticles exhibited H_c of 75, 2, and 1 Oe, respectively. The M_r of pure nanoparticles was 15 emu/g; the doped nanoparticles had zero M_r. Thus, the type of magnetic ordering in pure magnetite nanoparticles corresponds to the ferromagnetic ordering; whereas, the doped nanoparticles of magnetite are superparamagnetic.

Investigation of hyperthermic characteristics in magnetic nanoparticles. The heating characteristics (hyperthermic characteristics) of MNPs exposed to AMFs were measured using the LocalHyperThermLab Unit TOR 04/16 (OOO Nanomaterialy, Russia). The operating principle of the unit is based upon producing the magnetic field inside the solenoid with the coil, through which an electric current of the preset frequency is passed. The generator ensures the thermal stabilization of the compartment where the samples are held. Cuvettes filled with samples of colloidal suspensions of MNPs were placed in the compartment inside the solenoid. The unit allows producing a magnetic field with the amplitude ranging between 2 and 20 mT (~16 kA/m) and frequency 220–300 kHz. Sensitive IR detectors were used to detect the suspension temperature in the cuvette. The appearance and diagram of the experimental LocalHyperThermLabUnit TOR 04/16 are shown in Fig. 5.

The calorimetric studies of the MNPs' aqueous dispersions were conducted with the concentrations of 1.5 mg mL under exposure to an AMF with an amplitude of 20 mT and frequency of 218.9 kHz. The starting temperature 25°C in the chamber for the samples was maintained using a thermostat over the duration of the entire experiment. After exposure to an AMF (20 mT, 218.9 kHz), the base temperature (T_{noise}) of the aqueous solutions without nanoparticles was 27°C for 20 min.

Applying an AMF to magnetic materials induces the dissipation of magnetic energy in the form of heat (thermal) energy. Depending on the physicochemical characteristics of the magnetic materials, the energy is transformed into heat through four different heat loss mechanisms: eddy currents (in magnetic particles >1 μm) (1), hysteresis losses (in multidomain magnetic particles, ranging in size from ~70–100 nm to 1 μm) (2), and relaxation losses (Néel and Brown relaxation in the single-domain and superparamagnetic nanoparticles) (3, 4). The relative contribution of each mechanism is primarily determined by the size of the magnetic particles, magnetic anisotropy, and the fluid's viscosity.

To assure the safety of the body's live tissues, their exposure to the AMF is restricted to meet the following medical limits on the parameters values: the frequency should remain within the range from 50 kHz to 10 MHz, while the amplitude with sufficient penetration depth should not exceed 18 kA/m [4].

The heating efficiency of the MNPs in the AMF is determined by the SAR or Specific Loss Power (SLP), which is given as the ratio of the dissipated heat power to the mass of the MNP by the formula

$$\mathrm{SAR} = \frac{P}{m_{\mathrm{MNP}}}. \quad (1)$$

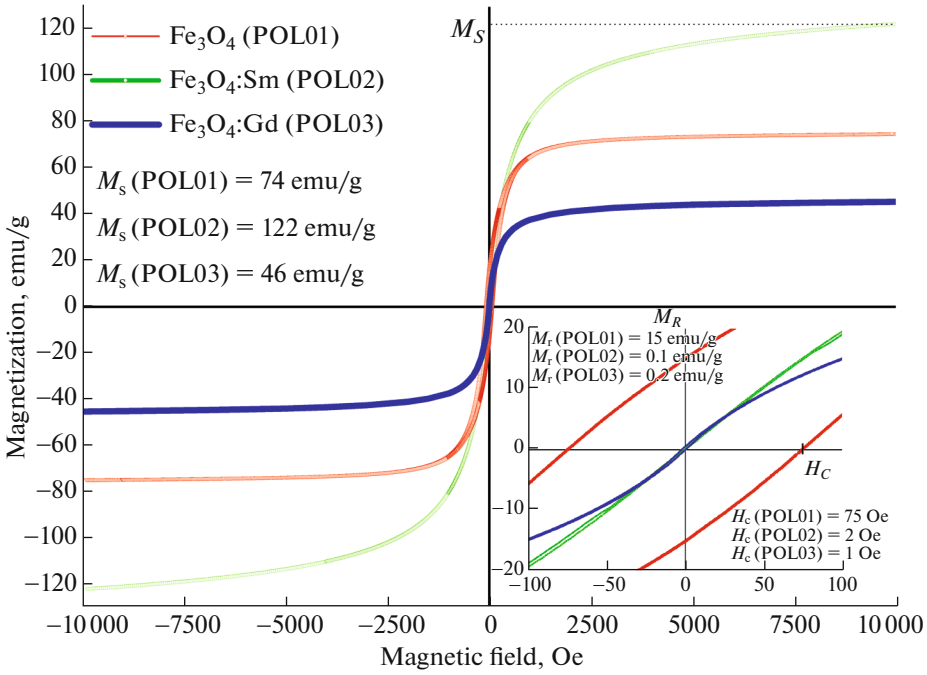

Fig. 4. (Color online) Loops of magnetic hysteresis of Fe_3O_4 (POL01), Fe_3O_4:Sm (POL02), and Fe_3O_4:Gd (POL03) nanoparticles coated with PEG-2000.

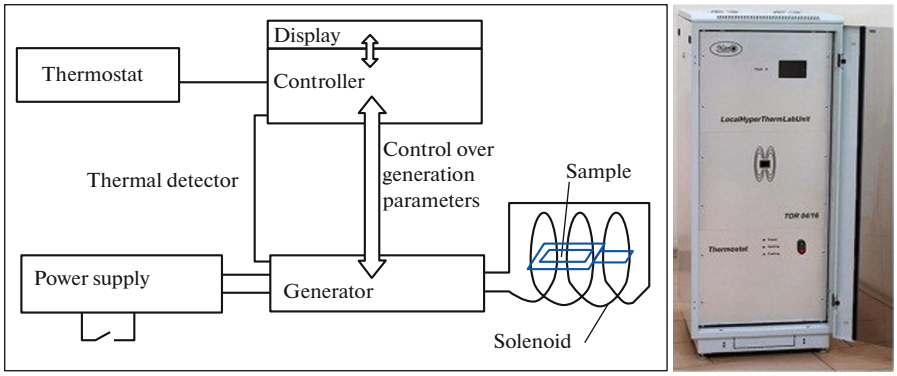

Fig. 5. (Color online) Diagram of the LocalHyperThermLabUnit TOR 04/16.

One of the limitations in the SAR representation include its dependence on frequency f and the square of the amplitude H^2 of AMF, which hampers direct comparison between the values reported in the literature due to the different parameters of the AMF applications. To solve this problem, we use the parameter of the ILP, as a result of which SAR is normalized by the strength and frequency of the alternating current [1]:

$$\mathrm{ILP} = \frac{\mathrm{SAR}}{fH^2}. \qquad (2)$$

However, the ILP representation is applicable only at a low field strength and alternating current at a low excitation frequency.

The technique for evaluating the heating characteristics of magnetic nanoparticles. The calorimetric approach is among the techniques commonly used to estimate the heating characteristics and assess the MNPs' magnetic hyperthermia properties. The approach involves recording the temperature rise in the sample over a particular time period when the MNPs are exposed to an AMF of a particular strength and frequency. Temperature measurements commonly involve fiber optical or IR sensors in combination with the magnetic induction system, consisting of a water-cooled coil connected to a high-frequency AMF generator. The samples are placed in a thermally insulated container to avoid heat loss during the measurement, while the SAR is calculated based on the

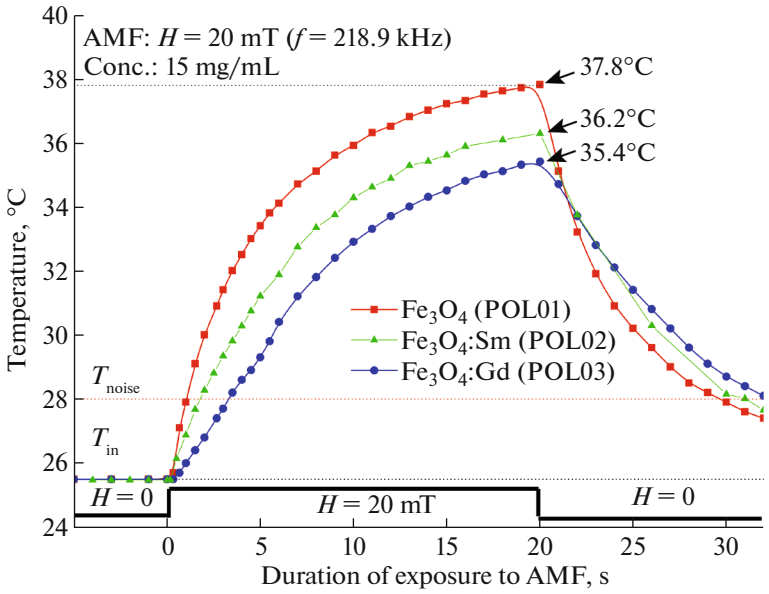

Fig. 6. (Color online) Dependence of the temperature of heating the aqueous dispersions of the synthesized nanoparticles (concentration of 15 mg/mL) on the duration of exposure to the AMF (218.9 kHz, 20 mT).

temperature derivative over time at time $t = 0$ from the formula

$$\mathrm{SAR} = \frac{CV_s}{m_{\mathrm{MNP}}}\left.\frac{dT}{dt}\right|_{t=0}, \quad (3)$$

where C is the specific heat capacity of the MNP suspension, V_s is the sample volume, m is the mass of the MNPs, dT/dt is the initial slope of the inflection in the time–temperature curve at the initial instant of exposure to an AMF.

The specific heat capacity C of the MNP suspension is calculated by the formula

$$C = C_{p,d}m_d + C_{p,\mathrm{MNP}}m_{\mathrm{MNP}}, \quad (4)$$

where $C_{p,d}$ is the specific heat capacity of the dispersion medium, $C_{p,\mathrm{MNP}}$ is the specific heat capacity of MNPs, m_d is the mass of the dispersion medium, and m_{MNP} is the mass of the MNPs.

The initial slope dT/dt ($t = 0$) of the time–temperature curve inflection at the initial instant of AMF exposure is calculated using the analytic approximate function $T(t)$:

$$T(t) = T_{\mathrm{in}} + \Delta T_{\max}\left(1 - e^{-\frac{t}{\tau}}\right), \quad (5)$$

where T_{in} is the initial temperature, $\Delta T_{\max}$ is the temperature's plateau value (at $t \to \infty$), and τ is the heating time constant. We can estimate $\Delta T_{\max}$ and the heating time constant τ, which corresponds to the time when the instant temperature value reaches ~63% of the terminal heating temperature of the magnetic fluid. After a time interval of 5τ, the system can be considered to attain a stable state close to $\Delta T_{\max}$.

The MNPs' heating rate at the instant is given by the equation

$$\nu = \left.\frac{dT}{dt}\right|_{t=0} = \frac{\Delta T_{\max}}{\tau}. \quad (6)$$

In addition, this value determines the angle of the linear heating of the MNPs under an adiabatic process.

The expression for a linear rise in the temperature $T(t)$ below is valid only for an adiabatic system:

$$T(t) = T_{\mathrm{in}} + \nu t. \quad (7)$$

The calorimetric approach was utilized to calculate the heating characteristics (SAR and ILP). The heating characteristics (hyperthermic characteristics) of the synthesized nanoparticles exposed to AMF were measured using the LocalHyperThermLabUnit TOR 04/16 (OOO Nanomaterialy, Russia).

Figure 6 illustrates the dependences of the heating temperature of the aqueous dispersion of the pure and doped rare-earth elements (Sm and Gd) of the MNPs for 20 min of the application of the AMF (218.9 kHz, 20 mT). The measured experimental data $T(t)$ are approximated using formula (4), from which the characteristics of the magnetic hyperthermia, such as the maximum heating temperature, heating rate, SAR, and ILP, were calculated. The calculated characteristics are presented in Table 2. During 20 min of exposure to the AMF, the aqueous dispersion of Fe_3O_4 nanoparticles (POL01) is heated to 37.8°C, whereas the aqueous dispersions of the doped MNPs are heated to a lesser extent (36.2°C (POL02) and 35.4°C (POL03)). The SAR and ILP values are the highest (11.5 W/g and 0.23 nH m^2/kg) for Fe_3O_4 (44.1 nm)

Table 1. Physicochemical and hyperthermic characteristics of a number of pure and doped nanoparticles of magnetite

Chemical composition	Description	Size of magnetic nucleus, nm	Parameters of AMF	M_S, emu/g	SAR, W/g	ILP, nH m^2/kg	Literature
Fe_3O_4	Coprecipitation, coated with PEG	10	25 mT, 112 kHz	60	8.4	0.2	[12]
$Mn_{0.4}Fe_{2.6}O_4$	Coprecipitation, coated with PEG	15	25 mT, 112 kHz	72	46	1.0	[12]
$Zn_{0.4}Fe_{2.6}O_4$	Coprecipitation, coated with PEG	11	25 mT, 112 kHz	66	25.1	0.6	[12]
$Mn_{0.2}Zn_{0.2}Fe_{2.6}O_4$	Coprecipitation, coated with PEG	12	25 mT, 112 kHz	81	4.2	0.1	[12]
$Co_{0.6}Fe_{2.4}O_4$	Hydrothermal synthesis, without coating	8	6 kA/m, 330 kHz	58.44	117.12	9.86	[13]
$Co_{0.6}Fe_{2.4}O_4$	Hydrothermal synthesis, without coating	9	6 kA/m, 330 kHz	31.76	58.56	4.93	[14]
$Y_{0.01}Fe_{2.99}O_4$	Without coating	13	16 kA/m, 413 kHz	69	194	1.85	[14]
$Gd_{0.02}Fe_{2.98}O_4$	Synthesized in the presence of dextran	13	246 Oe (~20 kA/m), 52 kHz	65.67	36	1.73	[15]
Fe_3O_4	Solvothermal synthesis, coated with PEG	44.1	20 mT, 218.9 kHz	74	11.5	0.23	Present study
$Sm_{0.033}Fe_{2.967}O_4$	Solvothermal synthesis, coated with PEG	14.4	20 mT, 218.9 kHz	122	8.2	0.15	Present study
$Gd_{0.058}Fe_{2.942}O_4$	Solvothermal synthesis, coated with PEG	17.7	20 mT, 218.9 kHz	46	5.7	0.1	Present study

Table 2. Hyperthermic characteristics of the synthesized nanoparticles

Sample	Composition	ΔT_{max}, °C	τ, min	$\nu = \Delta T_{max}/\tau = (dT/dt)t = 0$, °C/min	SAR, W/g	ILP, nH m^2 kg^{-1}
POL01	Fe_3O_4	12.01	4.82	2.492	689.1	7.87
POL02	Fe_3O_4:Sm	12.73	7.16	1.778	491.96	5.62
POL03	Fe_3O_4:Gd	12.77	10.27	1.243	343.7	3.92

MNPs coated with PEG and are lower for the doped (Sm and Gd) nanoparticles (8.2 W/g and 0.15 nH m^2/kg for (POL02) and 5.7 W/g and 0.1 nH m^2/kg for (POL03), respectively). The ILP values of magnetite nanoparticles (POL01) are consistent with the results of other studies on magnetite nanoparticles, whereas the doped (Sm and Gd) MNPs exhibit smaller values (Tables 1, 2) [12–15]. Table 3 shows the values of the parameters used to calculate the hyperthermic characteristics.

Table 3. Values of the parameters used for SAR calculation

	Fe_3O_4, including the doped NPs	Water
C_M, J/(mol K)	153.2	75.27
M, g/mol	231.54	18
C_{mass}, J/(g K)	0.66	4.18
m, mg	0.005	0.33

$C = C_{dispersion}m_{dispersion} + C_{MNP}m_{MNP} = 4.18 \times 0.33 + 0.66 \times 0.005 = 1.3827$ J/K; $C/m_{MNP} = 276.54$ J/(g K); SAR = 276.54ν; ILP = SAR/(fH^2) (where $f = 218900$ Hz, $H = 0.02$ T; $fH^2 = 87.56$).

Thus, we arrive at the conclusion that the synthesized pure nanoparticles and the nanoparticles doped by rare-earth elements (Sm and Gd) feature strong hypothermic characteristics and are suitable for application in the local magnetic hyperthermia.

CONCLUSIONS

The iron oxide-based superparamagnetic nanoparticles (Fe_3O_4) were obtained using the solvothermal synthesis. Both the pure Fe_3O_4 nanoparticles and the nanoparticles doped by samarium and gadolinium

were studied in order to compare their characteristics that are important for the local magnetic hyperthermia. The obtained materials were investigated using X-ray diffraction, X-ray fluorescence, vibrating-sample magnetometry, electron microscopy, and electron diffraction. The nanoparticles were shown to feature the crystal structure of magnetite and average size of about 22 nm, as well as superparamagnetic characteristics at room temperature. The nanoparticles' hyperthermic characteristics obtained in the AMF proved to be promising for application for the local hyperthermia in oncology.

FUNDING

This work was supported by the Russian Scientific Foundation, project no. 19-73-10069.

CONFLICT OF INTEREST

The authors declare that they have no conflicts of interest.

REFERENCES

1. P. Das, M. Colombo, and D. Prosperi, Colloids Surf., B **174**, 42 (2019).
2. D. Ortega and Q. A. Pankhurst, Nanoscience **1**, 60 (2013).
3. E. A. Périgo, G. Hemery, O. Sandre, et al., Appl. Phys. Rev. **2**, 41302 (2015).
4. S.-H. Noh, S. H. Moona, T.-H. Shina, et al., Nano Today **13**, 61 (2017).
5. A. E. Deatsch and B. A. Evans, J. Magn. Magn. Mater. **354**, 163 (2014).
6. Zh. Shaterabadi, Gh. Nabiyouni, and M. Soleymani, Prog. Biophys. Mol. Biol. **133**, 9 (2018).
7. S. S. S. R. Kumar and F. Mohammad, J. Adv. Drug Deliv. Rev. **63**, 789 (2011).
8. Z. Hedayatnasab, F. Abnisa, and W. M. A. Wan Daud, J. Mater. Des. **123**, 174 (2017).
9. E. C. Abenojar, S. Wickramasinghe, J. Bas-Concepcion, and A. C. S. Samia, J. Mater. Int. **26**, 440 (2016).
10. S. Laurent, S. Dutz, U. O. Häfeli, and M. Mahmoudi, Adv. Colloid Interface Sci. **166**, 8 (2011).
11. Sh. Ibrahim, H. Shokrollahi, and S. Amiri, J. Magn. Magn. Mater. **324**, 903 (2012).
12. L. Bissoli de Mello, L. C. Varanda, F. A. Sigoli, and I. O. Mazali, J. Alloys Compd. **779**, 698 (2018).
13. Z. E. Gahrouei, S. Labbaf, and A. Kermanpur, Phys. E (Amsterdam, Neth.) **116**, 113759 (2019).
14. P. Kowalik, J. Mikulski, A. Borodziuk, et al., J. Phys. Chem. C **124**, 6871 (2020).
15. P. Drake, H.-J. Cho, P.-S. Shih, et al., J. Mater. Chem. **17**, 4914 (2007).
16. H. Shi, P. Zhang, S.-S. Li, and J.-B. Xia, J. Appl. Phys. **106**, 023910 (2009).

Translated by E. Kuznetsova